Top Catal (2012) 55:747–756
DOI 10.1007/s11244-012-9862-7

ORIGINAL PAPER

# Hydrogenation of Carbon Dioxide on Rh, Au and Au–Rh Bimetallic Clusters Supported on Titanate Nanotubes, Nanowires and $TiO_2$

**M. Tóth · J. Kiss · A. Oszkó · G. Pótári · B. László · A. Erdőhelyi**

Published online: 25 July 2012


**Abstract** Supported gold, rhodium and bimetallic rhodium-core–gold-shell catalysts were prepared. The supports were $TiO_2$ as well as titanate nanotube and nanowire formed in the hydrothermal conversion of titania. The catalytic properties were tested in the $CO_2$ hydrogenation at 493 K. The amount and the reactivity of the surface carbonaceous deposit were determined by temperature-programmed reduction. The surfaces of the materials were characterized by X-ray photoelectron and low-energy ion scattering spectroscopy (LEIS). The surface forms during the catalytic reaction were identified by DRIFT spectroscopy. On the XP spectra of bimetallic catalysts the existence of highly dispersed gold particles could be observed besides the metallic form on all supports. Small Rh particles could also be identified on the titanate supports. LEIS spectra demonstrated that Rh-core–Au-shell particles formed, since no scattering from Rh was detected. The main product of $CO_2$ hydrogenation was $CH_4$ on all catalysts. IR spectra revealed the existence of CO and formate species on the surface. In addition, a new band was observed around 1,770 $cm^{-1}$ which was assigned as tilted CO. It is bonded to Rh and interacts with a nearby the oxygen vacancy of the support. Agglomeration of highly dispersed Rh was observed on bimetallic samples induced by reaction or reactant.

**Keywords** $CO_2$ hydrogenation · Titania nanowire · Titania nanotube · Core–shell structure · Gold · Rhodium

M. Tóth · J. Kiss · A. Oszkó · G. Pótári · B. László · A. Erdőhelyi (✉)
Department of Physical Chemistry and Material Science, University of Szeged, H-6720 Szeged, Aradi vértanúk t. 1, Szeged, Hungary
e-mail: erdohely@chem.u-szeged.hu

## 1 Introduction

One-dimensional nanostructures have been in the focus of the material science community for more than a decade now [1]. High-aspect-ratio $TiO_2$ and titanate nanoobjects are intensively studied at present because of their promising photoelectrical [2, 3], biomedical [4], and hydrogen storage properties [5, 6]. Gold-containing titania nanotubes were found to display higher activity in the photo-oxidation of acetaldehyde [7], the water–gas shift reaction [8], and CO oxidation [9] than the Degussa P-25 catalyst. Recently gold, rhodium and their coadsorbed layers were prepared on titanate nanowires and nanotubes and characterized by different surface science tools [10, 11]. XP measurements clearly pointed to the existance of highly dispersed state of gold stabilized on titanate nanowire and to a lesser extent on the nanotube. High resolution TEM study showed that while gold particles with diameter of 1.5–5 nm were distributed both inside and outside the nanotubes. In contrast, larger particles (10–70 nm) were only found on the external surface of the tube [7]. An atomically-dispersed state was observed for Au atoms complexed to oxygen vacancies on $TiO_2$(110) at low temperature [12].

In the presence of Rh on titanate nanocomposites it was found that, for appropriate Au and Rh coverages, the Au almost completely covers the Rh nanoparticles. It has also been observed earlier that Rh significantly changed the morphology and topology of Au on $TiO_2$(110) surface [13, 14]. STM and LEIS experiments revealed that at proper Au and Rh coverage Rh-core–Au-shell structure dominates. Interestingly, this kind of structure is not resistant against reaction components or reaction products. The LEIS data strongly support the phenomenon that CO induces a reconstruction of the core–shell structure. Rh preferentially segregates to the surface to form Rh-CO bond [15]. This

process may imply the migration of Rh or Au atoms within the clusters or on the surface of the cluster. A similar phenomenon was observed recently in the cases of bimetallic Au–Pt clusters on $TiO_2$(110) [16] and a Au–Pd bimetallic model catalyst [17].

The hydrogenation of $CO_2$ was studied extensively on different noble metal catalysts, among them Rh, which has been shown to be one of the most effective metals [18]. It was found that the support exerted a marked influence on the specific activity the Rh. The most effective support was $TiO_2$ and the least effective one was $SiO_2$ [19, 20]. Mainly methane was formed in the reaction with selectivities in some cases higher than 95 % [19]. Trovarelli et al. [21] found $C_1$–$C_6$ hydrocarbons in the $CO_2 + H_2$ reaction on $Rh/TiO_2$ and the product distribution was shown to follow Anderson–Schulz–Flory statistic. When hydrogenation of $CO_2$ was carried out on supported Rh at higher pressure (10 atm), not only methane but also methanol was also detected [22]. It was found that $Rh/TiO_2$ reduced at low temperature (533 K) exhibited high activity and low methanol selectivity. The activity change with reduction temperature was suggested to result not only from the change in the surface area of metal but also from the change in the electronic state of Rh [22]. The initial rate of $CO_2$ hydrogenation significantly increased with increasing reduction temperature up to 673 K but decreased drastically in a few seconds time-on-stream. The promotion effect of the reduction temperature was explained by the formation of oxygen vacancies on the perimeter of the $Rh/TiO_2$ interface, which can be re-oxidized by the adsorption of $CO_2$ and $H_2O$ [23]. The effect of oxygen vacancies on the rate of $CO_2$ hydrogenation was also demonstrated in the case of $Rh/CeO_2$ and $CeO_2$-promoted $Rh/SiO_2$ [24, 25].

The catalytic hydrogenation of $CO_2$ has been investigated as a function of the electric properties of the $TiO_2$ support [26, 27], induced by doping $TiO_2$ with cations lower- and higher-valencies. It was demonstrated that variation of the electric conductivity of $TiO_2$ influences the catalytic properties of Rh. The turnover rate of methane formation increased significantly when less than 1 % $W^{6+}$ ions were incorporated into the $TiO_2$ thereby increasing its electric conductivity by one or two orders of magnitude [26]. Such changes resulted in the increase of the specific activity of $CO_2$ methanation by up to 24 times [26].

The effect of the particle size of Rh and other noble metals on the $CO_2 + H_2$ reaction has been also investigated. Results obtained on $Ru/TiO_2$ demonstrate that the reaction is structure sensitive i.e. the turnover frequency depends on crystallite size of the dispersed metallic phase. It increased by more than 1 order of magnitude with increasing Ru crystallite size from 2.1 to 4.3 nm [22].

Similar results were obtained at low temperature (408–423 K) on $Rh/Al_2O_3$. Large particles were more active, whereas at higher temperature no significant difference could be detected [28]. The catalytic properties of Ru on different supports proved to be dependent on the metal dispersion; the lower the Ru dispersion the higher the reaction rate [29].

Relatively little attention was paid to the hydrogenation of $CO_2$ on Au catalysts [30–35]. Haruta and co-workers detected methanol [30, 31, 35] on $Au/TiO_2$ at 50 atm pressure. Smaller gold particles gave higher methanol productivity related to the gold surface area [30, 31]. When the pressure was 8 atm Au supported on $TiO_2$ was active in the hydrogenation of $CO_2$ to CO [35].

In the present paper we disclose our results with respect to the hydrogenation of carbon dioxide studied on Au, Rh and Au–Rh supported on nanocomposites including titanate nanowire (NW), nanotube (NT) and $TiO_2$.

## 2 Experimental

Titanate NWs and NTs were prepared by hydrothermal conversion of anatase $TiO_2$ as described elsewhere [36, 37]. Briefly, the nanostructures were prepared by mixing 2 g of anatase into 140 $cm^3$ 10 M aqueous NaOH solution until a white suspension was obtained, followed by aging in a closed, cylindrical, Teflon-lined autoclave at 400 K for 1–72 h while rotating the whole autoclave intensively at 60 rpm around its short axis. The reaction mixture then was washed with deionized water and neutralized with 0.1 M HCl acid solution to reach pH = 7. Finally the slurry was filtered and dried in air at 353 K. Au, Rh and their coadsorbed layers with different compositions were produced by impregnating titania NWs, NTs and $TiO_2$ (Degussa P25) with the mixtures of calculated volumes of $HAuCl_4$ (Fluka) and $RhCl_3{\cdot}3H_2O$ (Johnson Matthey) solutions to yield 1 wt% metal content. The impregnated powders were dried in air at 383 K for 3 h, and then oxidized at 573 K. Before each measurement the catalyst was heated in Ar flow up to 473 K and then oxidized in $O_2$ stream for 20 min. Afterward the reactor was flushed with He or Ar and heated up to 573 K. The sample was reduced at this temperature in $H_2$ flow for 60 min, then the reactor was flushed again with inert gas and cooled down to the desired temperature.

Titanate nanotubes are open-ended hollow tubular objects with outer diameters of 7–10 and 50–170 nm in length. They feature a characteristic spiral cross section composed of 4–6 wall layers. The typical diameter of their inner channel is 5 nm. Titanate NW represents the thermodynamically most stable form of sodium trititanate under the applied alkaline hydrothermal conditions. (Note that the post-synthetic neutralization step converts the original $Na_2Ti_3O_7$ into its hydrogen form without affecting the NW morphology.) Their diameter is 45–110 nm and

their length is between 1.8 and 5 μm. The specific surface area of titanate nanotubes is rather large ($\sim$185 $m^2$ $g^{-1}$) due to the readily accessible inner channel surface, whereas that of solid titanate NWs is $\sim$20 $m^2$ $g^{-1}$. The BET surface of Degussa $TiO_2$ applied here was 50 $m^2$ $g^{-1}$.

Catalytic reactions were carried out in a fixed bed continuous-flow reactor (200 × 10 mm o.d.). The amount of catalysts used was usually about 0.1 g. The dead volume of the reactor was filled with quartz chips. The $CO_2/H_2$ ratio in the reacting gas mixture was 1:4. The flow rate of the reactant was 50 ml/min. Analysis of the product gases was performed with a Chrompack 9001 gas chromatograph using Porapak QS column. The products were detected simultaneously by TC and FI detectors.

The amount and the reactivity of surface carbon formed in the catalytic reactions during 80 min were determined by temperature-programmed reduction (TPR). The catalyst was heated at a linear rate of 15 K/min hydrogen as carrier gas. Products were analyzed by gas chromatography.

Infrared spectra were recorded with a Bio-Rad FTIR spectrometer equipped with diffuse reflectance attachment (Spectra-Tech) with $BaF_2$ windows with a wave number accuracy of ±4 $cm^{-1}$. Typically 32 scans were registered. The whole optical path was purged by $CO_2$- and $H_2O$-free air generated by a Balston purge gas generator. The catalysts were pre-treated as mentioned above then the $CO_2 + H_2$ (1:4 mixture) was introduced into the cell at the reaction temperature and the IR spectra were recorded. The same experimental conditions were used as in the catalytic measurements. All spectra were rated to the spectra of the catalysts pre-treated before the measurements.

XP spectra were taken with a SPECS instrument equipped with a PHOIBOS 150 MCD 9 hemispherical analyzer. The analyzer was operated in the FAT mode with 20 eV pass energy. The Al $K_\alpha$ radiation ($h\nu = 1486.6$ eV) of a dual anode X-ray gun was used as an excitation source. The gun was operated at the power of 210 W (14 kV, 15 mA). The energy step was 25 meV, electrons were collected for 100 ms in one channel. Typically five scans were summed to get a single high resolution spectrum. For binding energy reference the Ti $2p_{3/2}$ maximum (458.9 eV) was used. The same data were obtained when C 1s (adventitious carbon at 285.1 eV), or O 1s lattice oxygen (530.3 eV) was used as reference. A sample preparation chamber was directly connected to the measuring chamber to avoid the contamination of samples between each step. For spectrum acquisition and evaluation both manufacturer's (SpecsLab2) and commercial (CasaXPS, Origin) software packages were used.

A SPECS IQE 12/38 ion source was used for generation of low-energy ion scattering (LEIS) spectra. $He^+$ ions of 800 eV kinetic energy were applied at a low ion flux equal to 0.03 μA/$cm^2$, which was necessary to avoid the sputtering of surface. The incident angle was 55° (with respect to surface normal), and ions ejected along the surface normal were detected. The ion energies (LEIS) were measured by the same hemispherical energy analyzer as mentioned above.

## 3 Results and Discussion

### 3.1 Characterization of the Catalysts

Gold, rhodium and gold–rhodium supported on titanate NW and NT were characterized earlier in detail [10, 11, 15, 38]. The XP spectra of monometallic gold nanoclusters on titania NWs showed two peaks on the reduced sample for Au $4f_{7/2}$ at 83.7 eV (metallic state) and 85.6 eV [15]. The emission at 85.6 eV cannot be attributed to a kind of higher oxidation state because it was developed after hydrogen treatment at 573 K. This feature was attributed to gold atoms of nanoparticles with very small sized ("final-state" effect).

On Au supported on nanotube the intensity of the gold feature at 85.6 eV was less than on wire [10]. It is important to mention that this high binding energy peak was not observed in the case of other support such as on $Au/TiO_2$ [39] and $Au/Al_2O_3$ [40], where gold deposits were prepared by similar impregnation methods.

On the monometallic Rh/NW the dominant XP peak for Rh $3d_{5/2}$ appeared at 307.2 eV after pre-treatment of the catalyst. A careful deconvolution of the peak revealed some emission at 309.3 eV, presumably due to more dispersed nanoparticles. Very similar rhodium XP spectra were recorded on titanate nanotubes [11].

On the XP spectra of the bimetallic Au + Rh layer supported on titania nanowires and nanotubes, surprisingly, the emission for the higher energy peak of Au $4f_{7/2}$ at 85.6 eV corresponding to the atomically dispersed state [12] decreased significantly in the presence of Rh, and at the same time the emission for Rh $3d_{5/2}$ around 309.2 eV also diminished [38].

The samples were characterized by low-energy ion scattering spectroscopy (LEIS) which is an extremely sensitive method to the topmost layer. On monometallic systems the gold and rhodium $He^+$ scattering signals appeared at 753 and 707 eV, respectively. In the case of 0.5 % Au + 0.5 % Rh bimetallic nanocomposite, however, only the gold signal showed up [15]. The rhodium peak was just a bit higher than the noise level. It is very interesting that while the gold content is less (0.5 %) in the bimetallic system, the LEIS intensity of Au was higher than in the monometallic case with an Au content of 1 %. It means that a significant part of gold remained in well-dispersed state on titania wire, while the rest of it covered the rhodium [10].

Similar investigations were carried out in the case of $TiO_2$ supported samples (Fig. 1). After reducing the $Rh/TiO_2$ (Degussa P25) catalyst with hydrogen at 573 K for 1 h there was no sign of the reduction of $TiO_2$, the Ti $2p_{3/2}$ peak is located at 459.0 ± 0.1 eV characteristic of $Ti^{4+}$ state. The Rh 3d peaks were asymmetric after reduction, resembling to the shape of spectra taken on metallic rhodium. However, the Rh $3d_{5/2}$ binding energy was 307.4 ± 0.1 eV, which is slightly higher than the value usually reported for metallic rhodium (307.0 eV). The obvious explanation for this upward shift could be that there is another component in the Rh 3*d* spectrum envelope representing a more oxidized Rh species. We applied a peak fitting procedure using two doublets—one asymmetric for the metallic component and one symmetric for a possible oxidized component (Fig. 1b 1). The resultant composition showed that the existence of another rhodium component cannot be excluded with Rh $3d_{5/2}$ positioned at 309.6 ± 0.1 eV. This could well be the remainder of the $RhCl_3$ starting material, but its quantity is not more than 2–3 % of the whole rhodium content not sufficient to modify the peak position itself. The existence of some $RhCl_3$ is also supported by the presence of the Cl 2*p* signal with Cl $2p_{3/2}$ at 198.5 eV. So the reason for the upward shift of the spectral envelope maximum must be a different process, the interaction of the Rh particles with the $TiO_2$ support. Using the same energy reference the Ti $2p_{3/2}$ binding energy was measured to be the same in the bimetallic catalyst after reduction and also in the whole course of the reaction. Again there is no evidence of the reduction of titania. The Rh $3d_{5/2}$ envelope was located at 307.1 ± 0.1 eV, which is almost identical with the value accepted for pure metallic rhodium. The Rh 3*d* signal consists of one doublet with full width at half maximum less than measured for Rh 3*d* in $Rh/TiO_2$. Interestingly the Rh emission is rather symmetric (Fig. 1b).

The Au 4*f* envelope could be fitted with two doublets in all states of the sample (Fig. 1a). The more intense Au $4f_{7/2}$ component was located at 84.1 eV characteristic of metallic gold. The Au $4f_{7/2}$ binding energy of the other doublet was 85.5 ± 0.1 eV. One could argue that this may be the residue of the starting material, but we must take into account that the spectra were taken after reduction and it is not probable that the starting compound would survive. Instead, we think that this high binding energy component may be due to highly dispersed gold particles on the catalyst surface. The amount of this component is about 30 % after reduction. LEIS spectra taken with 800 eV He ions on this sample displayed a single peak around 750 eV that corresponds to scattering from gold. Neither the position, nor the intensity changed with the proceeding of the reaction. No emission from Rh was observed at 707–708 eV in the case of Au–Rh bimetallic system (Fig. 2).

The adsorption of hydrogen was also studied on these samples (Table 1). On supported gold samples hydrogen adsorption was not observed by using a pulse system. In spite of the Rh-core–Au-shell structure of the bimetallic system a significant amount of hydrogen was bonded to these catalysts though the Rh is covered by Au. Similar results were obtained in the case of CO adsorption. These observations can be explained by the segregation of Rh to the surface then adsorbing CO [15]. The adsorption of hydrogen on the bimetallic samples could be interpreted by the assumption that hydrogen could penetrate through the Au shell to Rh if the shell is not perfect.

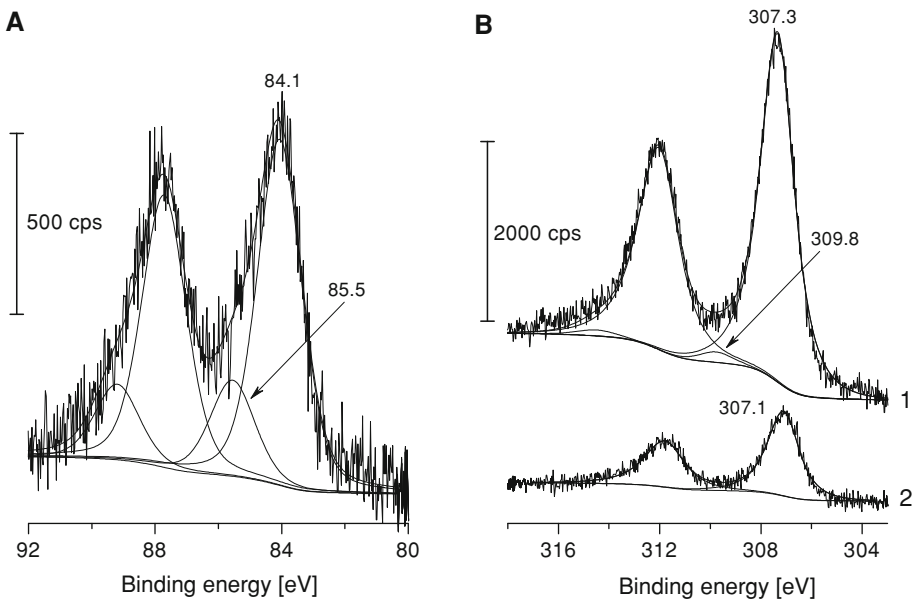


**Fig. 1** XP spectra of Au 4*f* (**a**) and Rh 3*d* (**b**) on pretreated $Rh/TiO_2$ (*1*) and $Au–Rh/TiO_2$ (*2*) catalyst

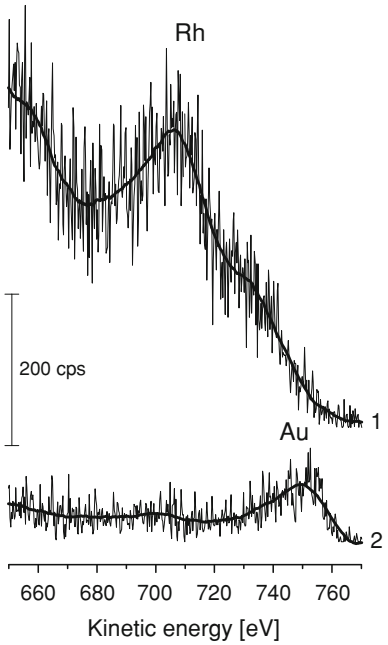


**Fig. 2** LEIS spectra of pretreated $Rh/TiO_2$ (*1*) and $Au–Rh/TiO_2$ (*2*) catalyst

### 3.2 Hydrogenation of $CO_2$

It was found earlier that $Rh/TiO_2$ exhibited the highest activity among different supported Rh catalysts [19, 23]. The selectivity of methane formation approached 99–100 %, only trace amount of ethane and CO were formed. It was also demonstrated [23] that on $Rh/TiO_2$ the initial rate of $CO_2$ hydrogenation significantly increased with increasing reduction temperature of the catalyst but the rate decreased drastically in few seconds time-on-stream.

In the present work we studied the reaction at lower temperature, 493 K, and higher space velocity than earlier to achieve relatively low conversion. The main product was $CH_4$ in all cases and CO was formed only on catalysts supported on nanotube. $C_2$ hydrocarbons were detected only in traces at 493 K. Some characteristic data are summarized in Table 1. The activity order of the supported Rh samples in the first minutes of the reaction decreased in the order $Rh/NW > Rh/TiO_2 > Rh/NT$. The conversion of $CO_2$ on Rh/NW decreased significantly in time but in the other cases the $CO_2$ consumption was relatively stable (Fig. 3). $Rh/TiO_2$ displayed the highest steady state activity. A drastic decrease in conversion was experienced when the bimetallic samples were used as catalysts but the activity order of the samples was the same. The supported Au samples were practically inactive in $CO_2$ hydrogenation. It seems that these observations contradict the results of Sakurai and Haruta [30, 31]. They studied the $CO_2 + H_2$ reaction using, among others, $Au/TiO_2$. At 523 K 18 % $CO_2$ conversion was found with CO and methanol as main products. The differences could be explained with the different experimental conditions. Sakurai and Haruta worked at high pressure (50 bar) and at relatively low space velocity (3,000 $h^{-1}$ ml $g^{-1}$). In our cases, in contrast, the pressure was atmospheric and the space velocity was one order of magnitude higher.

The activation energy of the reaction was determined from the temperature dependence of the $CH_4$ formation rate in the steady state. The values fell in the range 81–98 kJ/mol. These data are in good agreement with earlier findings [19]. There were no significant differences in the activation energies obtained on monometallic or bimetallic samples, with somewhat lower values for Au–Rh catalysts (Table 1).

**Table 1** Some characteristic data for hydrogenation of carbon dioxide on Rh, Au, Au–Rh bimetallic clusters supported on titanate nanotubes, nanowires and $TiO_2$

| Catalyst | Amount of adsorbed $H_2$ (μmol/g) | Conversion (%) | | $CH_4$ formation rate (μmol/g s) | | Turnover frequency ($s^{-1} \times 10^{-3}$) | $E_a$ (kJ/mol) | Σ C (μmol/g) |
|---|---|---|---|---|---|---|---|---|
| | | In 5 min | In 80 min | In 5 min | In 80 min | In 80 min | In 80 min | |
| $Rh/TiO_2$ | 7.9 | 6.9 | 6.7 | 4.9 | 4.4 | 278 | 98.3 | 78.8 |
| Rh/NW | 7.5 | 8.9 | 4.5 | 6.6 | 3.2 | 213 | 96.5 | 121.5 |
| Rh/NT | 4.1 | 1.4 | 1 | 0.8 | 0.5 | 61 | 88.4 | 132 |
| $Au–Rh/TiO_2$ | 2.4 | 3.3 | 2.5 | 2.2 | 1.5 | 312 | 81.3 | 38.9 |
| Au–Rh/NW | 5.0 | 1.5 | 1.3 | 1.1 | 0.9 | 90 | 85.3 | 98.6 |
| Au–Rh/NT | 2.5 | 0.4 | 0.4 | 0.2 | 0.1 | 20 | 98.8 | 215.7 |
| $Au/TiO_2$ | 0 | 0.0006 | 0.0002 | $3.7 \times 10^{-4}$ | $1 \times 10^{-4}$ | | | 17.2 |
| Au/NW | 0 | 0.005 | 0.09 | $3.5 \times 10^{-3}$ | $6 \times 10^{-4}$ | | | 11.6 |
| Au/NT | 0 | 036 | 0.098 | $8.3 \times 10^{-4}$ | $2.1 \times 10^{-4}$ | | | 3.0 |

$E_a$ Activation energy for $CH_4$ formation

Σ C Amount of surface carbon formed in the reaction at 493 K in 80 min

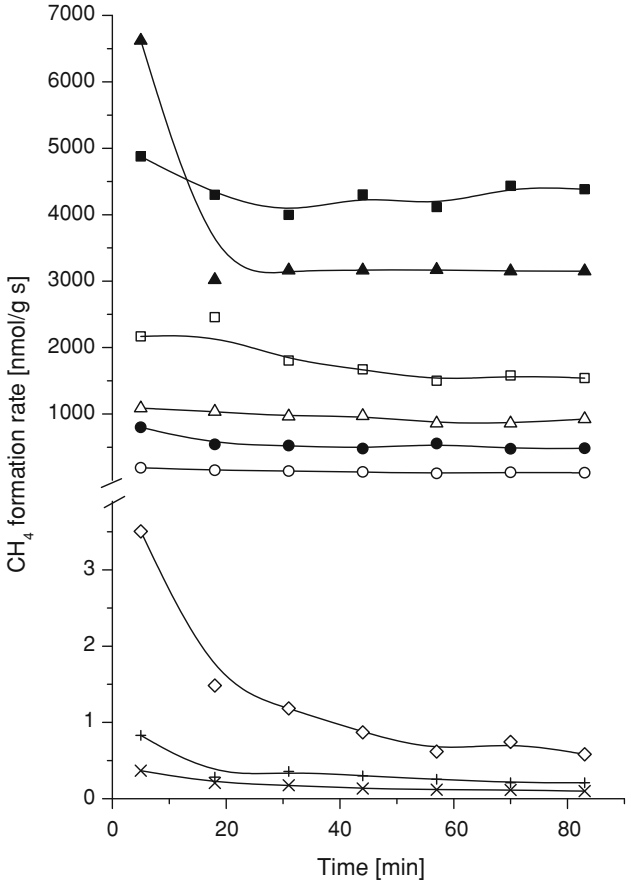


**Fig. 3** Rate of methane formation on $Rh/TiO_2$ (*filled square*), Rh/NW (*filled triangle*), Rh/NT (*filled circle*), $Au–Rh/TiO_2$ (*open square*), Au–RhNW (*open triangle*), Au–Rh/NT (*open circle*), $Au/TiO_2$ (*times symbol*), Au/NW (*open diamond*), AuNT (*plus sign*) catalysts at 493 K

The turnover rate of $CH_4$ formation (the rate related to the number of surface Rh atoms determined from hydrogen adsorption) was also calculated (Table 1.) The activity order of the samples in these cases was the same as mentioned above. The $TiO_2$-supported samples show the best activity whereas the nanotube supported catalysts exhibited the lowest efficiency. Interestingly, the highest turnover rate was found on $Au–Rh/TiO_2$ which was more active than the clean $Rh/TiO_2$ (Table 1). This observation could be explained by the effect of Au on Rh, but the increase of the turnover rate on bimetallic samples was found only on $Au–Rh/TiO_2$. Consequently, this explanation is probably irrelevant. Earlier it was found that the methanation of CO and $CO_2$ on dispersed noble metals is structure sensitive [41, 42]. For example the specific activity of Rh in $CO_2$ methanation decreased by a factor of 2.3 with increasing Rh crystallite size from 1.4 to 5.1 nm. This effect was explained by the assumption that the key step in the reaction seems to be favored at the edge and corner sites of the metal crystallites [42]. It is possible that we could also explain the increased activity of $Au–Rh/TiO_2$ with a similar structure effect.

To determine the amount of deposited carbon the reaction was performed at 493 K for 80 min and the reactor was flushed with Ar stream and cooled down to 340 K. The Ar gas was switched to hydrogen, the catalyst was heated with 15 K/min rate up to 1,100 K and the hydrocarbon formation was registered. Methane and especially on $Au/TiO_2$ and Au/NW ethane evolution were detected. The existence of different carbonaceous deposits on the catalysts is well illustrated by the TPR spectra in Fig. 4. Nearly the same features were found in all other cases. On Rh containing samples a small portion of surface carbon was hydrogenated to methane at 400–550 K and this was followed by a high temperature peak above 600 K. Similar TPR curves were found when the surface carbon was produced in the decomposition of methane at 523 K and only the ratio of the two peaks were different [43]. The low and the high temperature TPR peaks were found in the same temperature range irrespective of the metal or the support. It means that the reactivity of these species depends mainly on the composition and the structure of the carbonaceous deposit.

The amount of surface carbonaceous deposit formed during the reaction was determined from the TPR peak area (Table 1). Comparing the data obtained on different samples we have found that the amount of surface carbon depends not only on the metal but on the support, too. The effect of the metal on the amount of surface carbon could be explained by the different decomposition rate of surface species, such as formate ion or adsorbed CO, in the presence of different metals. The amount of deposited carbon decreased in the order of $NT > NW > TiO_2$, with the exception of supported Au samples (Table 1). In these

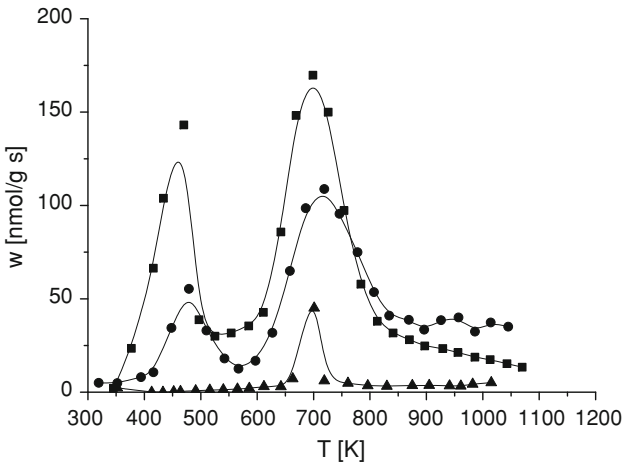


**Fig. 4** Temperature programmed reduction of carbonaceous deposit on Rh/NW (*filled square*), Au–Rh/NW (*filled circle*) and on Au/NW (*filled triangle*)

cases lower amounts of carbon were accumulated on the surfaces than on Rh containing samples (Fig. 4; Table 1) and there were no significant differences between the different supported Au catalysts.

### 3.3 Interaction of $CO_2$ with the Catalysts

The adsorption of $CO_2$ on clean Rh surface is a well-studied process, it is weak and nondissociative. Under ultrahigh vacuum (UHV) conditions $CO_2$, adsorbed at 100 K, completely desorbs below 300 K without dissociation. The results obtained in this field are summarized in two excellent reviews [44, 45]. On supported Rh the situation is basically different. In this case the dissociation of $CO_2$ occurs, but it also depends on the nature of the support. The most effective carrier was $TiO_2$, but even on these samples $CO_2$ dissociation was detected only above 373 K [46, 47]. It was found that on 5 % $Rh/TiO_2$ reduced at 673 K CO formation was observed already at 230 K, but when this sample was reduced at 473 K the dissociation of $CO_2$ was not detected until 290 K [48]. FTIR and TPD measurements revealed that $CO_2$ dissociation depends on the reduction temperature of the catalyst [23].

$CO_2$ adsorbs weakly on clean Au single crystal desorbing below 150 K ($T_p \sim 124$ K). The binding energy is greatly enhanced by the presence of potassium. At low K coverage the formed $CO_2^-$ species could dissociate into $CO_{(a)}$ and $O^-_{(a)}$ [49].

Figure 5 shows DRIFT spectra for different supported Rh and Au–Rh samples in a $CO_2$ flow at the reaction temperature, 493 K. On $Rh/TiO_2$ after 1 min the CO band was found at 2,047 $cm^{-1}$ and its intensity decreased in time. In the case of Rh supported on titanate nanotube absorption band characteristic for CO was observed at 2,033 $cm^{-1}$ and this band shifted to higher wave number in time. On Rh/NW an intensive band was observed at 2,062 $cm^{-1}$. The intensity of this band decreased also in time. Similar features were found on bimetallic samples only the band intensities were significntly lower. On supported Au samples we could not find any indication of CO band characteristic for $CO_2$ dissociation. The question is how the different behavior of the catalysts can be explained. Earlier it was found that the dissociation of $CO_2$ depends on the reduction degree of the $Rh/TiO_2$ catalyst [23]. This observation supports the speculation that the oxygen vacancies produced by the reduction of the catalysts promotes the dissociation of $CO_2$. When the sample was reduced at higher temperature the higher amount of defects formed resulted in the higher dissociation rates [23]. If this train of thought is continued we may suppose that the reduction of nanotube as support is negligible, or the tube contains some residue such as water which reoxidized the oxygen vacancies formed during the pretreatment.

### 3.4 Infrared Spectra Registered During the Catalytic Reaction

The infrared spectra registered in the DRIFT cell during the $CO_2$ hydrogenation showed that on Rh/NT (Fig. 6) and on Rh/NW (Fig. 7) from the beginning of the reaction an absorption band was present on the spectra in the CO region at 2,045 and 2,049 $cm^{-1}$, respectively. The intensities and the positions of these bands did not change significantly during the catalytic reaction. On Rh/NT a shoulder on the former peak was also observed at about 1,960 $cm^{-1}$. In this case bands were detected at 1767, 1640 $cm^{-1}$ and a weak band at 1,568 $cm^{-1}$ (Fig. 6.). On Rh/NW absorptions at 1775–1765, 1628, 1557–1555, and 1379 $cm^{-1}$ were found (Fig. 7). On $Rh/TiO_2$ intensive absorption was detected at 2,049 $cm^{-1}$ and a weak band at 1,620 and 1,570 $cm^{-1}$. Similar spectral features were found when Au–Rh/NW (Fig. 6), Au–Rh/NT (Fig. 7), and Au–$Rh/TiO_2$ were used as catalyst, only the intensities of the CO bands and on Au–Rh/NT the band at 1,770 $cm^{-1}$ were weaker.

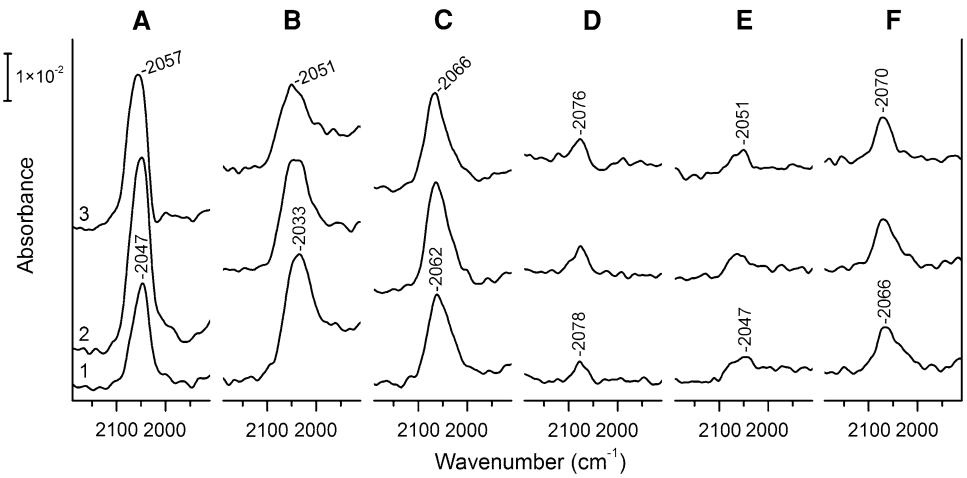


**Fig. 5** Infrared spectra registered during $CO_2$ adsorption on $Rh/TiO_2$ (**a**), Rh/NT (**b**), Rh/NW (**c**), Au–$Rh/TiO_2$ (**d**), Au–Rh/NT (**e**), Au–Rh/NW (**f**) at 493 K in the 1st (*1*), 3rd (*2*), and 5th minutes (*3*)

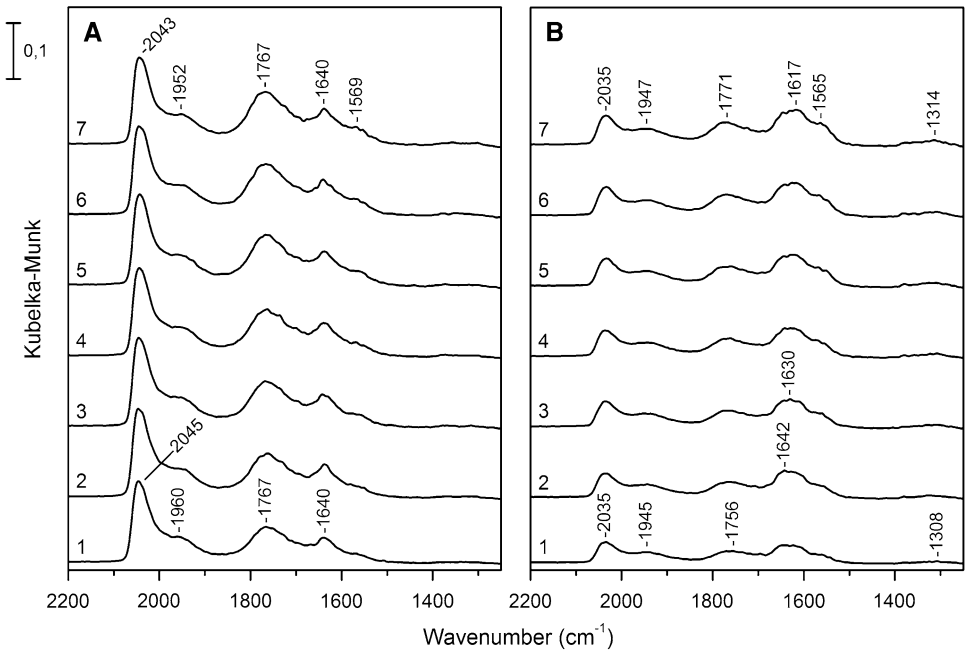


**Fig. 6** Infrared spectra registered during $CO_2 + H_2$ reaction at 493 K on Rh/NT (**a**) and Au–Rh/NT (**b**) in the 1st (*1*), 3rd (*2*), 5th (*3*), 10th (*4*), 30th (*5*), 60th (*6*), 120th minutes (*7*) of the reaction

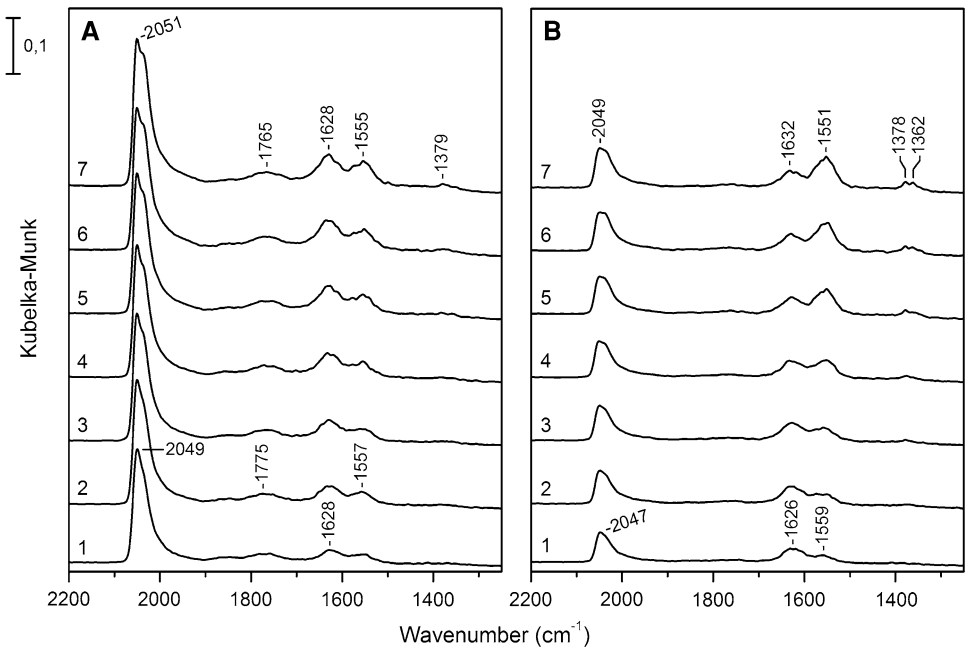


**Fig. 7** Infrared spectra registered during $CO_2 + H_2$ reaction at 493 K on Rh/NW (**a**) and Au–Rh/NW (**b**) in the 1st (*1*), 3rd (*2*), 5th (*3*), 10th (*4*), 30th (*5*), 60th (*6*), 120th minutes (*7*) of the reaction

The bands detected between 1,550–1,570 $cm^{-1}$ and 1,379 $cm^{-1}$ could be assigned as asymmetric and symmetric vibrations of the OCO group of formate species [50]. The absorption found at about 1,620 $cm^{-1}$ could be attributed to water formed in the reaction. The other bands below 1,700 $cm^{-1}$ are due to different carbonates bonded to the supports.

The $CO_2 + H_2$ interaction has been studied previously [46, 51] on different supported Rh catalysts; adsorbed CO and formate species were identified. The spectral feature of adsorbed CO formed in the $CO_2 + H_2$ reaction differed basically from that observed during the adsorption of gaseous CO; the doublet due to the twin structure $Rh(CO)_2$ was missing and the linearly bonded CO absorbed at lower frequencies. It was supposed that Rh carbonyl hydride was formed [23, 46, 51]. The adsorption of gaseous CO on the same samples resulted in the same spectra as found earlier: linearly bonded CO absorbing at 2,070 $cm^{-1}$ and the twin structure at 2,097 and 2,033 $cm^{-1}$ were detected on Au–Rh/NW [38]. During the $CO_2 + H_2$ reaction an intensive band was detected in all cases between 2,040 and 2,045 $cm^{-1}$ which could be assigned to the formation of Rh carbonyl hydride as found earlier.

The assignation of the band at 1,760–1,770 $cm^{-1}$ is more complicated. The absorption band of C=O group of formaldehyde adsorbed on $Rh/TiO_2$ appears at lower wave number at about 1,727 $cm^{-1}$ [52], although the vibration frequency of –C=O groups in the gaseous HCOOH is at 1,770 $cm^{-1}$ [53]. However, the band found in our cases can not be assigned to this feature because it was stable when the samples were flushed with He after the catalytic reaction.

Low wave number CO (under 1,790 $cm^{-1}$) has been observed in CO adsorption on Mn, La, Ce, Fe promoted $Rh/SiO_2$ catalysts [54–56]. It was suggested that Lewis acid sites caused the downward shift of CO ligand wave number by the interaction of the Lewis acid with the oxygen atom of CO. The carbon atom of chemisorbed CO bonded to Rh atom and the oxygen tilted to the metal ion [54–56]. In our cases we are inclined to assign the band at about 1,770 $cm^{-1}$ to such type of tilted CO which is bonded to the Rh and interacts with the oxygen vacancy of the titanate support.

### 3.5 XP Spectra Registered on Used Catalyst

When Rh was supported on $TiO_2$ nanotube, the Rh 3*d* signal could be fitted with two doublets after reduction (Fig. 8). The first, asymmetric doublet with Rh $3d_{5/2}$ positioned at 306.9 eV corresponds to metallic rhodium. The binding energy of Rh $3d_{5/2}$ in the other, symmetric component was 308.1 eV earlier attributed to highly dispersed Rh. The Rh signal always contained the above components in all stages of the reaction with the $CO_2 + H_2$ gas mixture. The situation was similar on the Au + Rh bimetallic catalyst after reduction. Though the signal intensity was only half compared to the monometallic sample, an obvious shoulder could be detected on the high binding energy side of the Rh 3*d* signal with Rh $3d_{5/2}$ positioned at 308.2 eV. In the reaction with $CO_2 + H_2$ gas mixture the position and intensity of the component attributed to metallic Rh did not change, but the intensity of the high binding energy highly dispersed component gradually decreased and nearly completely vanished after 60 min of the reaction. The Au 4*f* spectrum could be also fitted with two doublets. The more intense Au $4f_{7/2}$ was found at 83.4 eV and corresponds to metallic gold, while the less intense component at 85.3 eV is again identified with highly dispersed gold. This composition remained practically unchanged throughout the reaction; the amount of highly dispersed gold is approximately one-fifth of the metallic state. The LEIS spectra showed a single Rh peak at 708 eV on the $Rh/TiO_2$ nanotube sample. Similarly to the Degussa P 25 supported sample, no emission from Rh could be seen on the bimetallic sample in either state and only a weak Au peak was detected around 750 eV.

Both the XPS and LEIS spectra detected on Rh/NW were rather similar to those detected on nanotube support after reduction. However, the peak attributed to highly dispersed Rh was less intense on the Au + Rh sample supported on titanate NW. The disappearance of the high binding energy Rh $3d_{5/2}$ component is unambiguous. Tentatively it can be attributed to the reaction or reactant induced agglomerization.

## 4 Conclusion

The simultaneous deposition of gold and rhodium on titania and titanate nanowire and nanotube supports resulted in

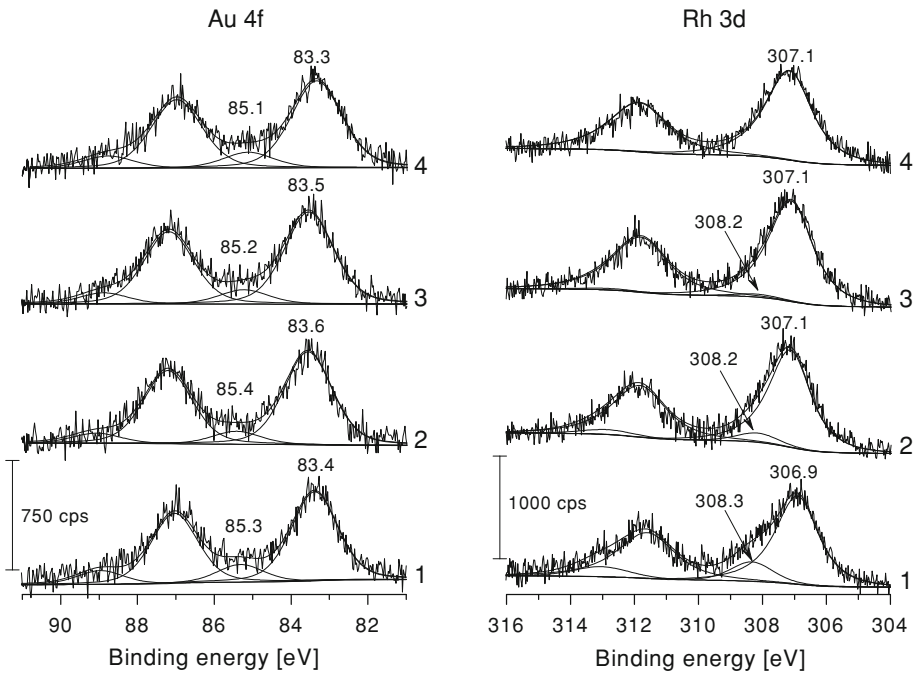


**Fig. 8** XP spectra of Au 4*f* and Rh 3*d* on Au–Rh/NT reduced sample (*1*), in the 5th (*2*), 30th (*3*) and 120th minutes (*4*) of $CO_2 + H_2$ reaction

the formation of Rh-core–Au-shell structures as evidenced by LEIS measurements. Besides these particles highly dispersed gold can be found on the surface of the support. The existence of such small particles is demonstrated by the high binding energy Au 4f components of the XPS spectra taken on all supports. On Rh/NT and Rh/NW catalysts the peak fitting procedure revealed the possible existence of highly dispersed Rh particles. Neither support showed the signs of reduction after catalytic application. Both kinds of gold were detectable throughout the treatment, but the intensity of highly dispersed Rh drastically decreased on nanotube support after 60 min of the reaction. The $CO_2 + H_2$ reaction followed at 493 K on these catalysts by gas chromatography showed that the main product was $CH_4$ in all cases. A minor amount of CO formed on nanotube supported catalysts. Supported gold samples were practically inactive. The amount and reactivity of surface carbonaceous deposit depended not only on the metal but also on the support. DRIFT spectra revealed the existence of CO and formate groups on the Rh/NW, Rh/NT and on all bimetallic catalysts. Additionally, a new band around 1,770 $cm^{-1}$ was identified which was attributed to tilted CO that is bonded to Rh and interacts with a nearby oxygen vacancy of the support.

**Acknowledgments** Financial support of this work by the Hungarian Science Foundation (OTKA contract number K 76489), TÁMOP-4.2.1/B-09/1/KONV-2010-000 and HU RO/0901/090/2.2.2 project is gratefully acknowledged.

## References

1. Xia Y, Yang P, Sun Y, Wu Y, Mayers B, Gates B, Yin Y, Kim F, Yan H (2003) Adv Mater 15:353
2. Mor G, Shankar K, Paulose M, Varghese O, Grimes C (2005) Nano Lett 5:191
3. Kubota S, Johkura K, Asanuma K, Okouchi Y, Ogiwara N, Sasaki K, Kasuga T (2004) J Mater Sci Mater Med 15:1031
4. Kavan L, Kalbac M, Zukalova M, Exnar I, Lorenzen V, Nesper R, Graetzel M (2004) Chem Mater 16:477
5. Bavykin D, Lapkin A, Plucinski P, Friderich J, Walsh F (2005) J Phys Chem B 109:19422
6. Huang R, Chung F, Kelder E (2006) J Electrochem Soc 153:1459
7. Malwadkar S, Gholap R, Awante S, Korake P, Chaskar M, Gupta N (2009) Photochem Photobiol A Chem 203:24
8. Idakiev V, Yuan Z, Tabakova T, Su B (2005) Appl Catal A Gen 281:149
9. Akita T, Okumura M, Tanaka K, Ohkuma K, Kohyama M, Koyanagi T, Date M, Tsubota S, Haruta S (2005) Surf Interface Anal 37:265
10. Kukovecz Á, Pótári G, Oszkó A, Kónya Z, Erdőhelyi A, Kiss J (2011) Surf Sci 605:1048
11. Oszkó A, Pótári G, Erdőhelyi A, Kukovecz Á, Kiricsi I, Kiss J (2011) Vaccum 85:1114
12. Lee S, Fan C, Wu T, Anderson S (2005) Surf Sci 578:5
13. Óvári L, Bugyi L, Majzik Zs, Berkó A, Kiss J (2008) J Phys Chem C 112:18011
14. Óvári L, Berkó A, Balázs N, Majzik Zs, Kiss J (2010) Langmuir 26:2167
15. Kiss J, Óvári L, Oszkó A, Pótári G, Tóth M, Baán K, Erdőhelyi A (2012) Catal Today 181:163
16. Tenney S, Ratliff J, Roberts C, He W, Ammal S, Heyden A, Chen D (2010) J Phys Chem C 114:21652
17. Gao F, Wang Y, Goodman D (2010) J Phys Chem C 114:4036
18. Solymosi F, Erdőhelyi A (1980) J Mol Catal 8:471
19. Solymosi F, Erdőhelyi A, Bánsági T (1981) J Catal 68:371
20. Henderson M, Worley S (1985) J Phys Chem 89:1417
21. Trovarelli A, Mustazza C, Dolcetti G, Kaspar F, Grazioni M (1990) Appl Catal 65:129
22. Inoue T, Iizuka T, Tanabe K (1989) Appl Catal 46:1
23. Novák E, Fodor K, Szailer T, Oszkó A, Erdőhelyi A (2002) Topics Catal 20:107
24. Trovarelli A, de Leitenburg C, Dolcetti G, Llorca J (1995) J Catal 151:111
25. de Leitenburg C, Trovarelli A, Kapar A (1997) J Catal 166:98
26. Solymosi F, Tombácz I, Koszta J (1985) J Catal 95:578
27. Zhang Z, Kladi A, Verykios X (1994) J Catal 148:737
28. Karelovie A, Ruiz P (2012) Appl Catal B Environ 113–114:237
29. Kowalczyk Z, Stolecki K, Rarog-Pilecka W, Miskiewicz E, Wilczkowska W, Karpinski Z (2008) Appl Catal A Gen 342:35
30. Sakurai H, Haruta M (1995) Appl Catal A Gen 127:93
31. Sakurai H, Haruta M (1996) Catal Today 29:361
32. Sloczynski J, Grabowski R, Kozlowoka A, Olnewksi P, Stoch J, Skozypek J, Lachowska M (2004) Appl Catal A Gen 278:11
33. Koeppel R, Baiker A, Wokaun A (1991) J Chem Soc Faraday Trans 87:2821
34. Wambach J, Baiker A, Wokaun A (1999) Phys Chem Chem Phys 1:5071
35. Sakurai H, Tsubata S, Haruta M (1993) Appl Catal A Gen 102:125
36. Horváth E, Kukovecz Á, Kónya Z, Kiricsi I (2007) Chem Mater 19:927
37. Kukovecz Á, Hodos M, Horváth E, Radnóczi G, Kónya Z, Kiricsi I (2005) J Phys Chem B 109:17781
38. Kiss J, Oszkó A, Pótári G, Erdőhelyi A (2012) Vaccum 86:594
39. Kiss J, Németh R, Koós Á, Raskó J (2009) J Nanosci Nanotechnol 9:3828
40. Raskó J, Koós Á, Baán K, Kiss J (2007) React Kinet Catal Lett 90:187
41. Ojeda M, Rojas S, Boutonnet M, Pérez-Alonso F, García-García F, Fierro J (2004) App Catal A Gen 274:33
42. Panagiotopoulou P, Kondarides D, Verykios X (2011) Ind Eng Chem Res 50:523
43. Erdőhelyi A, Cserényi J, Solymosi F (1993) J Catal 141:287
44. Solymosi F (1991) J Mol Catal 65:337
45. Freund H, Roberts M (1996) Surf Sci Rep 25:225
46. Solymosi F, Erdőhelyi A, Bánsági T (1981) J Chem Soc Faraday Trans 77:2645
47. Henderson M, Woorley S (1985) J Phys Chem 89:392
48. Raskó J, Solymosi F (1994) J Phys Chem 98:7147
49. Farkas A, Solymosi F (2009) J Phys Chem C 113:19930
50. Raskó J, Kecskés T, Kiss J (2004) J Catal 224:261
51. Solymosi F, Erdőhelyi A, Kocsis M (1980) J Catal 65:428
52. Raskó J, Kecskés T, Kiss J (2004) J Catal 226:183
53. Simanouchi T (1972) Tables of molecular vibrational frequencies consolidated vol. 1. National Bureau of Standards, Washington, DC
54. Ichikawa M, Fukushima T (1985) J Phys Chem 89:1564
55. Stevenson S, Lisitsyn A, Knözinger H (1990) J Phys Chem 94:1576
56. Chuang S, Stevens R, Khatri R (2005) Top Catal 32:225